Analysis of information content on hypertemporal UAV images

Hipertemporális UAV felvételek információtartalmának elemzése

Lóránt Biró [1*], József Berke [2], Kristóf Kozma-Bognár [3] and Veronika Kozma-Bognár[2]

[1] *Budapest Business University, Faculty of Commerce, Hospitality and Tourism, biro.lorant@uni-bge.hu*

[2] *Dennis Gabor University, Drone Technology and Image Processing Scientific Lab; kozma.bognar.veronika@gde.hu, berke.jozsef@gde.hu*

[3]*Hungarian University of Agriculture and Life Sciences, Festetics György Doctoral School*

**Correspondence: biro.lorant@uni-bge.hu*

Abstract: Today, the data provided by drones extremely useful information for professionals. The processing of large data sets collected by UAVs, on the other hand, may require different methodological elements based on the properties of the sensors placed in each camera system. The sensors placed on the carrier devices can significantly influence not only the collection of data, but also the evaluations appropriate for the given purpose. The data sets created by the sensors can be characterized by different geometric, spectral and temporal resolutions for each camera system. We can characterize the information content of the spectral layers of the Bayer-type CFA filter (Color Filter Array) and Global Shutter sensors by calculating information-theoretic entropy. If we have different spectral, geometric, and temporal data series available after the recording, the processing can be done by processing the data series separately or together. In the case of aerial photographs with different characteristics, data fusion procedures can also be used in the data processing process, which poses many challenges for remote sensing specialists. Properly performed data fusion can further increase the potential of the data. In our article, we present the information content-based processing of our environmental protection aerial surveys carried out in the sample area of Kis-Balaton. During image processing, we performed geodesic-based and pattern-matching-based integration of the data, the results of which are also presented with an entropy-based analysis of the images. We extended our investigations to the most frequently used image classification procedures in practice, and we also present the analysis of the error matrices related to the analysis of the result images of the procedures and the obtained Kappa indices. All of these were done in the manner described above because they do not require unique solutions and farmers, or users can do them even with basic knowledge.

Keywords*: UAV, hypertemporal, multispectral, plant protection, classification*

Összefoglalás: Napjainkban a drónok által szolgáltatott adatok rendkívül hasznos információkat szolgáltatnak a szakemberek számára. A UAV-k által gyűjtött nagy méretű adatsorok feldolgozása viszont eltérő módszertani elemeket igényelhetnek az egyes kamerarendszerekben elhelyezett érzékelők tulajdonságai alapján. A hordozó eszközökön elhelyezett érzékelők nemcsupán az adatok gyűjtését, hanem az adott célnak megfelelő kiértékeléseket is jelentősen befolyásolhatják. Az érzékelők által létrehozott adatsorokat az egyes kamerarendszerekre vonatkozóan eltérő geometriai, spektrális és időbeli felbontás jellemezheti. Információelméleti entrópia számításával jellemezhetjük a Bayer típusú, CFA filtert tartalmazó (Color Filter Array) és a Global Shutter érzékelők spektrális rétegeinek

információtartalmát. Amennyiben a felvételezést követően eltérő spektrális, geometriai és időbeli adatsorok állnak rendelkezésünkre, a feldolgozás történhet az adatsorok külön-külön vagy ezek együttes feldolgozásával. Az eltérő tulajdonságú légifelvételek esetében az adatfeldolgozás folyamatában adatfúziós eljárásokat is alkalmazhatunk, mely számos kihívást jelent a távérzékeléssel foglalkozó szakemberek számára. A megfelelően elvégzett adatfúzió tovább növelheti az adatokban rejlő lehetőségeket. Cikkünkben bemutatjuk a Kis-Balaton mintaterületén végzett, környezetvédelmi célú légifelvételezéseink információtartalom alapú feldolgozását. A képfeldolgozás során elvégeztük az adatok geodéziai alapú és mintaillesztés alapú integrálását, melynek eredményeit a felvételek entrópia alapú elemzésével is bemutatjuk. A vizsgálatainkat kiterjesztettük a gyakorlatban leggyakrabban alkalmazott képosztályozó eljárásokra is, továbbá bemutatjuk az eljárások eredményképeinek elemzéséhez kapcsolódó hibamátrixok elemzését és a kapott Kappa-indexeket. Mindezeket azért végeztük a fentiekben ismertetett módon, mert nem igényelnek egyedi megoldásokat és a gazdák vagy felhasználók alapismeretek mellett is elvégezhetik.

***Kulcsszavak**: drón, hipertemporális, multispektrális, növényvédelem, osztályozás*

1. Introduction

Light is electromagnetic radiation that can be broken down into different wavelength ranges. In the VIS (Visible, i.e., red [R], green [G], blue [B]) range, the colour bodies found in the vegetation are primarily reflected, meaning that the condition of the vegetation can be well examined with this range. The NIR (Near Infrared) range is generally used in agriculture for testing the fitness status of vegetation, similarly to the RedEdge band, but the latter is not sensitive to atmospheric conditions and soil reflectance but is sensitive to canopy characteristics and on the chlorophyll content (Clevers et al., 2001; Kozma-Bognár, 2012).

A non-negligible question of spectral tests is how many channels, i.e. bands, the used sensor can simultaneously record at a moment in time. From this point of view, we distinguish between multi- and hyperspectral recording. The difference between the two methods is on the one hand in the number of simultaneously recorded bands (multispectral: 4-20 bands, hyperspectral: >20 bands; Council of the European Union, 2009), and on the other in the width of the band ranges. In the case of the multispectral method, the bandwidths are usually large (50-120 nm), while in the case of hyperspectral recording they are much smaller, even 1 nm (Kozma-Bognár, 2012). As a result, the spectral resolution of the images is also much higher in the case of hyperspectral images, since the spectrum is continuous, while with the multispectral method the resulting spectrum consists of discrete band ranges.

While the use of hyperspectral sensors is common in satellite remote sensing (Bácsatyai and Márkus, 2001; Mucsi, 2013; Lillesand et al., 2015), it is not yet widespread in drone technology. This is due to the high cost and weight of hyperspectral camera systems on the one hand, and the limited size of the payload that drones can carry on the other. Despite this, more and more manufacturers are developing ever smaller size and weight hyperspectral camera systems that can be mounted on UAVs (Unmanned Aerial Vehicles, i.e., "drone"), thanks to their wide applicability - and their more cost-effective use compared to satellites (Adão et al., 2017; Nex et al., 2022). In contrast, many manufacturers currently produce high-quality multispectral camera systems especially for UAVs (e.g., Micasense, Parrot, Sentera, Yusense), which usually contain 6 channels: in addition to RGB, RedEdge (~717 nm) and NIR (~842 nm) bands.

Using RGB and/or RedEdge, as well as the NIR range, several indices have been created, which are primarily used to examine vegetation (Lussem et al., 2018; Solymosi et al., 2019; Feng et al., 2021). The scope of the study does not allow for a detailed presentation of the

indices, so only the NDVI and NDRE indices need to be mentioned due to the methodology used.

Both the normalized red border index (NDRE; 1) and the normalized vegetation index (NDVI; 2) provide information on the health status, or fitness, of the vegetation. While the NDVI index considers the R (i.e., red) band, the NDRE index uses the RedEdge band instead of the R band based on the following formula:

$$NDRE = (NIR - RedEdge) / (NIR + RedEdge) \quad (1)$$

$$NDVI = (NIR - RED) / (NIR + RED) \quad (2)$$

In the case of certain plants (e.g., corn), in the late life stage, the upper leaves absorb more of the red-light range, so the lower leaves do not contribute to the calculation of the NDVI index, i.e., the index will not show the real state. This is eliminated by the NDRE index, by calculating with the RedEdge band instead of the red band, since the light range is utilized to the same extent by the lower leaves of the plant, so the calculated NDRE index will already show a real picture (Carlson and Ripley, 1997; Maccioni et al., 2001).

By the temporal resolution of the image recordings, we mean the frequency of image creation. Like spectral resolution, multi- and hyper-temporal recording can also be distinguished in this case. Both cases have in common that the frequency of recording is much higher than the sampling frequency required for observing temporal processes – i.e., half the frequency of the examined temporal process (Shannon theorem: Shannon, 1948). Time is the fourth dimension; it differs from the x, y, z (spatial) dimensions in that it is asymmetric – that is, it only flows in one direction – and is difficult to imagine (we see the effects of the passage of time, but do not perceive it directly; Piwowar et al. 1998). The difference between the multi- and hypertemporal methods is the frequency of recording. There is no unified position regarding the frequency, for example Kleynhans (2011) draws the line between multi- and hypertemporal recording at a frequency of 8-30 days. Based on the recommendation of Piwowar et al. (1998), multitemporal data can be processed if the following three requirements are met:

1. It should be univariate (recording of the same parameter at different times).
2. Include time slices, each of which contains the same area (image pixels and resolution must match perfectly).
3. They should be radiometrically consistent (i.e., the images should be made with the same sensors).

In our opinion, the above can be completed with general user knowledge. However, as previously highlighted - Enyedi et al. (2016) and Vastag et al. (2019), in the case of devices where we work with sensors that do not contain discrete bands, and a significant part of the VIS sensors of UAV devices contain such, i.e., Bayer-type sensors, the actual data content of the image and its reliability are determined by the imaging algorithms. However, these differences can even exceed 100% - Enyedi et al. (2016). These data cannot be improved with subsequent (geometric, atmospheric or radiometric) corrections either, as they are procedures prior to their implementation. If, on the other hand, we create a single image band from the data of the entire Bayer sensor, then the data can be corrected, but we cannot create indexes, and most known classification methods cannot be used because of the single band. After taking the above into account, as well as comparing discrete-non-discrete sensors, we worked on the basis of reflectance values during the tests.

2. Materials and Methods

2.1. Presentation of applied technology

The images were made with a DJI Phantom 4 rotary-wing quadcopter drone, the camera parameters of which are as follows:

- Camera type: FC300X
- Sensor type: Sony EXMOR 1/2.3"
- Effective pixel: 12.4 M
- Image size: 4000 x 3000 px
- FOV: 94°
- Focal length: 20 mm
- Aperture: f/2.8
- Shutter speed: 8-1/8000 s

The Phantom 4 type drone only has an RGB sensor, however, the Sentera company produces accessories that can be used to connect various Sentera camera systems to DJI drones. Thus, two types of Sentera camera systems can be connected to the used Phantom 4 drone, with which either NDVI vegetation index (includes 625 nm red and 850 nm NIR band) or NDRE index (720 nm RedEdge and 840 NIR) in addition to NDVI the camera can record. Thus, recording will not be single axis, but RGB on a separate axis and NDVI and/or NDRE on a separate axis. The latter, i.e., the "dual" NDVI, NDRE camera system, was connected to the Phantom 4 drone, so the drone took NDVI and RE (only RedEdge instead of NDRE index) images of the area at the same time in addition to RGB images.

2.2. Presentation of study area

The investigated area is located on the Kis-Sziget of the Zimány part of the Kis-Balaton landscape, which is no longer an independent island and has an area of ~4200 m^2 (Figure 1). Kis-Balaton itself is part of the Balaton Uplands National Park, which is highly protected, so you can only enter with a permit. The area - together with Lake Balaton - forms an independent ecological system, which is also unique in the world, and even enables the temporal examination of vegetation changes caused by climate change (Soós et al., 2014). Thus, the monitoring of vegetation with a UAV is increasingly becoming an indispensable method for research in this direction.

3. Applied methodology

The images were made with the DJI Phantom 4 drone mentioned in the previous chapter and its FC300X type RGB camera (resolution is 1969 x 4879), and the NDVI and RedEdge images (resolution is 2271 x 5619) were made with an NDVI, NDRE, RedEdge camera (Sentera Double 4K True) located on a separate axis – that is, as a kit that can be installed on the Phantom 4 drone. The images were taken in the year 2020, with an average frequency of 12 days, at the same time of the day, at an altitude of 100 m, and of course always from the same area. The dates are as follows: January 2, 15, 26, February 14, 29, March 10, 27, April 8, 18, 26, May 8, 18, 30, June 13, 24, July 6, 19, 30, August 9, 20, September 2, 11, 22, October 1, 19, 27, November 1. The images were taken by flying on the same route, during which average VIS – 44.08±1.19, NDVI – 22.81±1.62, RE – 22.78±1.67 images were taken. The images were taken with 70%/80% (Side/Frontal) overlap. The difference in the number of images between the two cameras was mainly caused by the different viewing angle, while the difference between the

flight times was due to the different weather conditions. The images were aligned with the Agisoft PhotoScan 1.4.3 program with factory default settings, separately for the RGB and separately for the Sentera sensor, image alignment - dense cloud – DEM - Orthophoto in order.

The photos taken (3 channels, counting 27 times, a total of 81 image files) were taken in raw, i.e., RAW (36-bit) format, which were converted into the lossless 16-bit TIFF image format, which is also lossless, but more suitable for further processing. After the conversion, the images were joined by channel, that is, the RGB, NDVI and RedEdge images were copied into one image file. We separated the RGB images based on the three bands (red, green, blue), so we created three more new image files, so a total of six new files were available, which contain 27-27 channels, where one channel means one image, following each other in chronological order. In other words, the images belonging to the same band were copied "to each other", so 27-channel TIFF images were created, where one channel represented one recording. In this case, the sequence lasted from 01/02/2020 to 11/01/2020, but from the point of view of the method, it does not matter which time (channel) is visible, that is, which recording is in the top position of the data cube.

The TIFF files joined by bands were further processed with ENVI (5.6.2) software, where the main purpose of the processing was the classification of the joined image files by bands. Since the classification was done using supervised methods, the first step was to select the known areas, i.e., the ROIs (Region of Interest). During the designation, we separated four types of vegetation: tall golden cane, sedge, reed, and shrub. Variations caused by phenological phases were not investigated in this work. In the sedge-reed areas, this is justified, but neither farmers/professionals with general preparation nor the factory-provided software solutions currently allow this. The tall golden cane and shrub parts were clearly separated in the area.

After the designation of the ROIs, the classification followed, for which we used two methods, the Maximum Likelihood (ML) and the Spectral Angle Mapper (SAM) method. Based on experience, Maximum Likelihood results in the most accurate classification, while the Spectral Angle Mapper method is effective when there are relatively many shadows in the image (Schowengerdt, 1997; Kozma-Bognár, 2012,). The prepared image files (RGB, NDVI, RE) (images from 27 to 27 times) were classified using the above two supervised methods.

We analysed the Overall Accuracy, which can be expressed as several pixels per image or as a percentage. When examining the accuracy of the results, it is also appropriate to compare the Commission/Omission and Producer Accuracy/User Accuracy values (Appendix 1.), and to consider the Kappa coefficient, which is an indicator of the match between the classification and the real values. A Kappa value of 1 indicates a perfect match, while a value of zero indicates no match (Richards-Jia, 2005). Table 2 summarizes the hit accuracies and Kappa values associated with each classification procedure. We created an error matrix to check the created classes, so it is possible to objectively compare the results of the classification of each band, and the matrix also reveals the relationships between the classes (Kevi, et al. 2023). For the objective evaluation of the error matrices, we used a multivariate statistical method - cluster analysis.

To examine the information content of each band, Shannon's entropy was calculated for each band at each time point (Shannon, 1948). With the help of this, it is possible to clearly see which band contains the largest information content (thus the most colour shades, which are important during classification), i.e., which band has the highest entropy value.

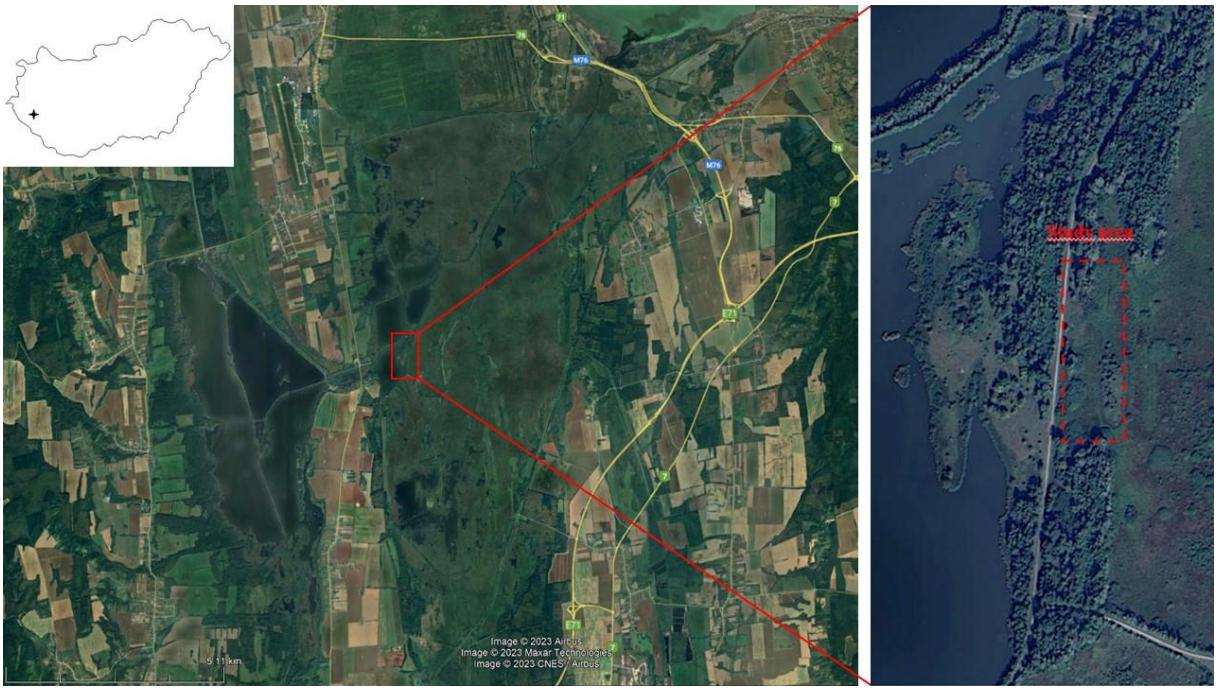

Figure 1. *Location of the study area (Kis-Sziget: red dotted area, projection WGS84)*

The vegetation of the area is characterized by sedges, reeds, and tall goldenrod, which is of adventitious North American origin, while the woody vegetation is mainly composed of various willows. These four vegetation types completely cover the investigated area, which can be separated from each other spectrally (VIS + NIR) and represent discrete pixels based on the resolution of the recordings. In terms of vegetation, the biggest problem is the presence and expansion of tall goldenrod. This weed species is characterized by the fact that, relatively quickly, it can form stable closed stands with few species in just four years, displacing the original, site-specific plant types (Pinke and Pál, 2005).

4. Results, evaluation

4.1. Comparison of classification methods

Comparing the image results of the classifications is difficult to perform and can lead to subjective interpretation, so the differences can be seen objectively on the error matrices. From both the classified images and the error matrices - as well as from Table 1 - the Maximum Likelihood (ML) method generally performed better than the Spectral Angle Mapper (SAM) method (see Appendix 1. for the Commission/Omission and Producer Accuracy/User Accuracy values). This is most striking when examining the aggregate accuracy values of the bands.

Table 1. Overall accuracy and Kappa coefficient of classes by band and method

Band	Method	Overall Accuracy	Kappa Coefficient
RGB	Maximum Likelihood	48.60	0.30
	Spectral Angle Mapper	40.64	0.18
R	Maximum Likelihood	82.67	0.76
	Spectral Angle Mapper	53.84	0.38
G	Maximum Likelihood	87.16	0.82
	Spectral Angle Mapper	60.09	0.46
B	Maximum Likelihood	79.56	0.72
	Spectral Angle Mapper	52.96	0.37
RedEdge	Maximum Likelihood	33.94	0.09
	Spectral Angle Mapper	26.24	0.02
NDVI	Maximum Likelihood	37.94	0.13
	Spectral Angle Mapper	36.09	0.09

If we compare the values of the individual groups within the bands, it is mostly significant only in the case of the R, G, B bands that the ML method gives better results than the SAM method. This statement is not entirely true for the classification results of the RGB, RE (RedEdge) and NDVI bands, it is also clearly visible from the comparison of the values of the aggregated accuracy.

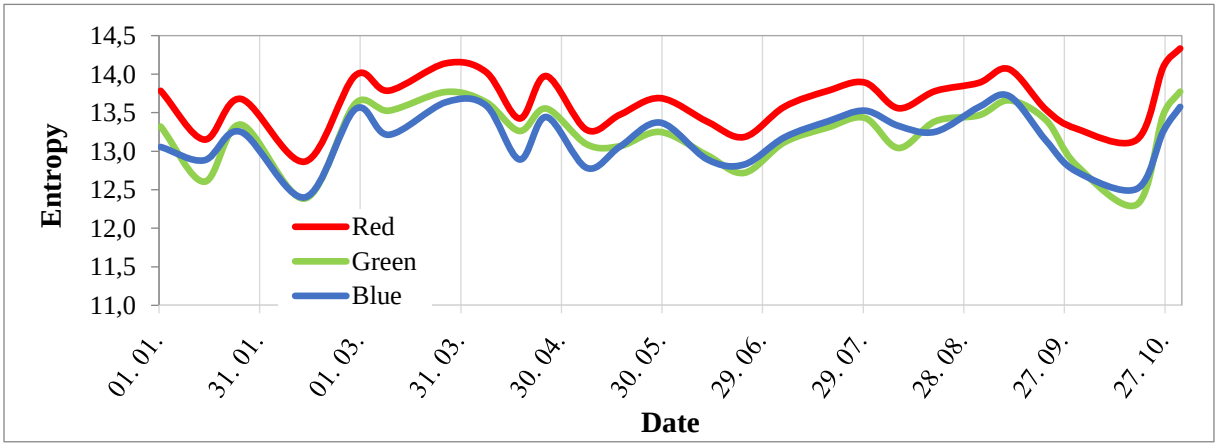

Figure 2. *Entropy values per band of RGB images*

Overall, the classification of the G (green) band using the ML method gave the most accurate results, although based on the entropy of the bands, the red band contains the most information (Figure 2), while the worst parameters were given by the classification of the RE band using

the SAM method. In terms of the classes, the golden point, which is important for the tests, can best be observed by classifying the G (green) band with the ML method.

4.2. Interpretation of results

It helps to interpret the results if we can decide whether the result is acceptable or not for a group classified with a specific band and method. In the previous chapter, we presented the results classified by the given method and band based on accuracies, so it can be said for each group whether the result is adequate or not. This evaluation - that is, whether a group is "good" or not - can also be examined objectively, namely with a multivariate statistical method, clustering. In this case, we know the producer's and user's accuracy, the probability of commission and omission from the class for each group. These provide the input data of the method, based on which we want to classify the group into reliable and unreliable categories, that is, we want to classify them into 2 clusters (k-means clustering).

As a result of the clustering, two groups were created, the general parameter values of which are shown in Table 2. Group 1 contains the band/method/ROI combinations that lead to bad results, since their accuracy is low (<37%), but the probability of commission and omission is high (>63%). On the other hand, Group 2 contains those band/method/ROI combinations that gave good results, as their accuracy is high (>75%) and the probability of commission and omission is low (<25%).

Table 2. Average parameter values of two groups obtained as a result of clustering

Group / Parameter	Producer's accuracy	User's accuracy	Commission	Omission
Group 1.	35.6	37.4	62.6	64.4
Group 2.	81.4	75.4	24.6	18.7

An important question is which band/method combinations belong to the identified groups, since this way it is possible to specify which of the above combinations should be used later, if we want to use hypertemporal images for classification. Figure 3 helps in this, based on which the above question can be clearly answered, so if we want to achieve adequate accuracy, one of the bands R, G, B must be used and classified using the Maximum Likelihood method. The reason for the accuracy of these three bands is probably the change in the green and red pigments of the vegetation during the vegetation period, the effect of which is reflected in the variance of the RGB values of the pixels - this is also shown by the entropy of the bands over time (Figure 2). This assumption is further supported by Figure 3, which shows that the classification of the images of the G (green) band gives the most accurate results.

In the case of the "underpowered" bands (RGB, RE, NDVI), a probable error factor may be that the RE, NDVI images were not located on the same axis as the other RGB, R, G, B bands. This also resulted in slips occurring between the images (the slippage of successive images at the same time was below 0.25%, but this error increased during the joint matching of the entire images recorded at 27 times), i.e., the area was not the same for every image (the resolution, of course, did not change). These slippages could also cause classification inaccuracies. However, the inaccuracy of the RGB images is certainly surprising, and the solution to this question requires further investigations.

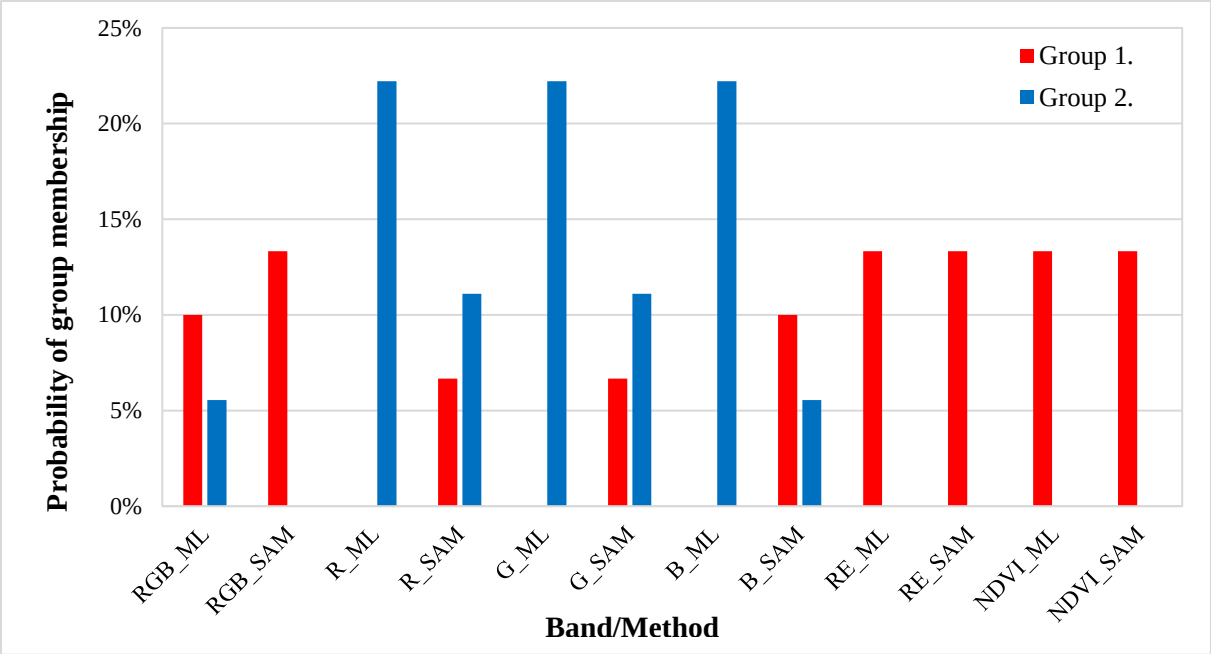

Figure 3. *Composition of groups obtained as a result of clustering based on band/method combinations*

5. Conclusions

Based on the conclusions drawn so far, it can be stated that RGB sensors are also partially suitable for vegetation monitoring studies using multitemporal images, namely, by evaluating the R band, adequate accuracy can be achieved, especially if the classification is carried out using the Maximum Likelihood method. It is important to point out that a perfect result can only be obtained by processing the panchromatic - that is, the images read directly from the sensor. The pixel values of RGB images contain data loss compared to the original recording, the extent of which we can only estimate, but this must be considered during interpretation.

When applying the methodology, it is worth paying attention to the recording of which time the topmost layer of the data cube contains, since this recording will be classified during processing. Of course, this also gives the possibility that if the recording of the data cube made at any time is placed in the top position, i.e., on the very first channel, then this recording is classified using the images made at all other times. In fact, this is where the efficiency of the method lies, that is, the classification is done using the images always made, so we get the most accurate classification possible (with the selection of the appropriate method).

When pre-processing the data, care must also be taken to ensure that the images are always taken from the same height and from the same area. In the case of multi-axis recording, this requirement is not fully met, so inaccuracies may occur during the classification (especially in the case of the SAM method), so it is more desirable to take single-axis images (e.g., using multitemporal sensors).

As a continuation of the work, after the methodological evaluation, it may be worthwhile to classify the images using the Maximum Likelihood method of the R band in such a way that the uppermost channel of the data cube is always a recording from a new time. In this way, a time series would essentially be created, with the help of which you can see the territorial changes of the goldenrod during the investigated vegetation period. This can lay the foundation for further nature conservation and intervention tasks, which would enable protection against the aggressively expanding adventive vegetation (in this case, tall goldenrod) within the territory of the Balaton-felvidéki National Park.

Acknowledgements

Project no. TKP2021-NVA-05 has been implemented with the support provided by the Ministry of Innovation and Technology of Hungary from the National Research, Development and Innovation Fund, financed under the TKP 2021 funding scheme.

References

Adão, T., Hruška, J., Pádua, L., Bessa, J., Peres, E., Morais, R., and Sousa, J. 2017. Hyperspectral Imaging: A Review on UAV-Based Sensors, Data Processing and Applications for Agriculture and Forestry. *Remote Sensing* **9** (11), 1110. https://doi.org/10.3390/rs9111110

Bácsatyai L., Márkus I. 2001. Fotogrammetria és távérzékelés. Kézirat, Sopron.

Carlson, T. N., and Ripley, D. A. 1997. On the relation between NDVI, fractional vegetation cover, and leaf area index. *Remote Sensing of Environment*. **62** (3), 241–252. https://doi.org/10.1016/s0034-4257(97)00104-1

Clevers, J. G. P. W., de Jong, S. M., Epema, G. F., van der Meer, F., Bakker, W. H., Skidmore, A. K., and Addink, E. A. 2001. MERIS and the red-edge position. *International Journal of Applied Earth Observation and Geoinformation*. **3** (4), 313–320. https://doi.org/10.1016/s0303-2434(01)85038-8

Enyedi, A. – Kozma-Bognár, V. – Berke, J. 2016. Comparison of imaging algorithms for remote sensing based on content and image structure, *Remote Sensing Technologies & GIS Journal.***6** (6), 464-475.

Európai Unió Tanácsa 2009. A Tanács 428/2009/EK rendelete a kettős felhasználású termékek kivitelére, transzferjére, brókertevékenységére és tranzitjára vonatkozó közösségi ellenőrzési rendszer kialakításáról. Az Európai Unió Hivatalos Lapja. L 134/1. https://eur-lex.europa.eu/legal-content/HU/TXT/HTML/?uri=CELEX:32009R0428&from=en#ntr1-L_2009134HU.01000101-E0001

Feng, H., Tao, H., Zhao, C., Li, Z., and Yang, G. 2021. Comparison of UAV RGB Imagery and Hyperspectral Remote-sensing Data for Monitoring Winter-wheat Growth. https://doi.org/10.21203/rs.3.rs-170131/v1

Kevi, A., Berke J., Kozma-Bognár V. 2023. Comparative analysis and methodological application of image classification algorithms in higher education. Journal of Applied Multimedia 1./XVIII./2023 https://doi.org/10.26648/JAM.2023.1.002.

Kleynhans, W. 2011. Detecting land-cover change using MODIS time-series data. PhD Thesis. University of Pretoria. Pretoria.

Kozma-Bognár V. 2012. Hiperspektrális felvételek feldolgozásának és mezőgazdasági alkalmazásának vizsgálata. PhD Értekezés. Pannon Egyetem Állat- és Agrárkörnyezet-tudományi Doktori Iskola. Keszthely

Lillesand, T., Kiefer, R.W., and Chipman, J. 2015. Remote Sensing and Image Interpretation. Wiley, USA.

Lussem, U., Bolten, A., Gnyp, M. L., Jasper, J., and Bareth, G. 2018. Evaluation of RGB-based vegetation indices from UAV imagery to estimate forage yield in grassland. *The International Archives of the Photogrammetry, Remote Sensing and Spatial Information Sciences.* **42** (3), 1215–1218. https://doi.org/10.5194/isprs-archives-xlii-3-1215-2018

Maccioni, A., Agati, G., and Mazzinghi, P. 2001. New vegetation indices for remote measurement of chlorophylls based on leaf directional reflectance spectra. *Journal of*

Photochemistry and Photobiology B: Biology. **61** (1–2), 52–61. https://doi.org/10.1016/s1011-1344(01)00145-2

Mucsi L. 2013. Műholdas távérzékelés: Elmélet és gyakorlat. Szegedi Tudományegyetem Természeti Földrajzi és Geoinformatikai Tanszék, Szeged.

Nex, F., Armenakis, C., Cramer, M., Cucci, D. A., Gerke, M., Honkavaara, E., Kukko, A., Persello, C., and Skaloud, J. 2022. UAV in the advent of the twenties: Where we stand and what is next. *ISPRS Journal of Photogrammetry and Remote Sensing*. **184**, 215–242. https://doi.org/10.1016/j.isprsjprs.2021.12.006

Pinke Gy., Pál R. 2005. Gyomnövényeink eredete, termőhelye és védelme. Alexandra, Pécs.

Piwowar, J. M., Peddle, D. R., and LeDrew, E. F. (1998): Temporal Mixture Analysis of Arctic Sea Ice Imagery: A New Approach for Monitoring Environmental Change. *Remote Sensing of Environment.* **63** (3), 195–207. https://doi.org/10.1016/s0034-4257(97)00105-3

Richards, J. A. and Jia, X. 2005. Remote Sensing Digital Image Analysis: An Introduction 4th Edition, Springer, Berlin. https://doi.org/10.1007/3-540-29711-1

Schowengerdt, R.A. 1997. Remote Sensing. Models and Methods for Image Processing, 3rd Edition, Academic Press, Boston

Shannon, C. 1948. A Mathematical Theory of Communication. *Bell System Technical Journal*. **27**. 379–423.

Solymosi, K., Kövér, G., and Romvári, R. 2019. The Development of Vegetation Indices: a Short Overview. *Acta Agraria Kaposváriensis.* **23** (1), 75–90. https://doi.org/10.31914/aak.2264

Vastag, V. K. – Óbermayer, T. - Enyedi, A. – Berke, J. 2019. Comparative study of Bayer-based imaging algorithms with student participation, *Journal of Applied Multimedia*. **14** (1), 7-12. https://www.jampaper.eu, https://doi.org/10.26648/JAM.2019.1.002

Appendix 1. Commission/Omission and Producer Accuracy/User Accuracy values of the ROI's

Blue - Maximum Likelihood				
Class	Producer Accuracy	User Accuracy	Comission	Omission
Reeds	71,17	72,04	27,96	28,83
Sedges	70,40	77,25	22,75	29,60
Goldenrod	90,26	86,32	13,68	9,74
Bush	88,05	80,27	19,73	11,95
Blue - Spectral Angle Mapper				
Class	Producer Accuracy	User Accuracy	Comission	Omission
Reeds	55,47	43,49	56,51	44,53
Sedges	34,56	53,20	46,80	65,44
Goldenrod	53,20	60,04	39,96	46,80
Bush	82,35	55,26	44,74	17,65

Green - Maximum Likelihood				
Class	Producer Accuracy	User Accuracy	Comission	Omission
Reeds	82,25	74,72	25,28	19,75
Sedges	81,00	85,91	14,09	19,00
Goldenrod	94,28	94,33	5,67	5,72
Bush	94,45	92,90	7,10	5,55
Green - Spectral Angle Mapper				
Class	Producer Accuracy	User Accuracy	Comission	Omission
Reeds	61,79	45,59	54,41	38,21
Sedges	33,28	58,81	41,19	66,72
Goldenrod	76,09	66,08	33,92	23,91
Bush	79,60	71,55	28,45	20,40

RedEdge - Maximum Likelihood				
Class	Producer Accuracy	User Accuracy	Comission	Omission
Reeds	34,26	34,58	65,42	65,74
Sedges	12,52	37,46	62,54	87,48
Goldenrod	73,23	33,99	66,01	26,77
Bush	7,37	24,13	75,87	92,63
RedEdge - Spectral Angle Mapper				
Class	Producer Accuracy	User Accuracy	Comission	Omission
Reeds	33,50	21,10	78,90	66,50
Sedges	40,97	34,82	65,18	59,03
Goldenrod	1,63	26,52	73,48	98,37
Bush	31,95	20,72	79,28	68,05

Red - Maximum Likelihood				
Class	Producer Accuracy	User Accuracy	Comission	Omission
Reeds	72,28	69,44	30,56	27,72
Sedges	76,85	80,99	19,01	23,15
Goldenrod	91,61	90,63	9,38	8,39
Bush	90,44	88,17	11,83	9,56
Red - Spectral Angle Mapper				
Class	Producer Accuracy	User Accuracy	Comission	Omission
Reeds	53,90	39,50	60,50	46,10
Sedges	25,66	54,14	45,86	74,34
Goldenrod	70,40	60,83	39,17	29,60
Bush	76,79	61,18	38,82	23,21

RGB - Maximum Likelihood				
Class	Producer Accuracy	User Accuracy	Comission	Omission
Reeds	16,14	37,61	62,39	83,86
Sedges	39,82	57,34	42,66	60,18
Goldenrod	76,86	48,99	51,01	23,14
Bush	55,56	43,62	56,38	44,44
RGB - Spectral Angle Mapper				
Class	Producer Accuracy	User Accuracy	Comission	Omission
Reeds	19,86	23,51	76,49	80,14
Sedges	52,27	49,95	50,05	47,73
Goldenrod	57,18	46,61	53,39	42,82
Bush	16,96	23,36	76,64	83,04

NDVI - Maximum Likelihood				
Class	Producer Accuracy	User Accuracy	Comission	Omission
Reeds	5,14	24,86	75,14	94,86
Sedges	58,69	41,83	58,17	41,31
Goldenrod	49,05	39,07	60,93	50,95
Bush	20,90	26,62	73,38	79,10
NDVI - Spectral Angle Mapper				
Class	Producer Accuracy	User Accuracy	Comission	Omission
Reeds	6,75	21,44	78,56	93,25
Sedges	55,03	40,14	59,86	44,97
Goldenrod	53,25	37,13	62,87	46,75
Bush	8,32	19,63	80,37	91,68